5.7. Summit, Greenland (7/31/09– 11/23/10)

This section describes quality control of solar data recorded by the SUV-150B spectroradiometer at Summit Camp, Greenland, between 7/31/09 and 11/23/10. Data of the period 7/31/09 – 12/31/09 were assigned to Volume 19; data of 2010 were assigned to Volume 20.

Of note, the system was removed from the "Green House" where it is normally located on 6/19/09 as the building needed to be raised above snow level, and re-leveled. The instrument was reinstalled at the end of July 2009. The first solar data after re-installation were measured on 7/31/09, the first day of the reporting period.

Changes in responsivity observed during the last years continued in 2009 and 2010. These changes are caused by variations in collector efficiency and PMT sensitivity. The chances are now well understood and were corrected during data processing. Residual variations in published data were assessed by comparing SUV-150B data with measurements of the co-located GUV-511 multi-filter radiometer and results of radiative transfer calculations, and are smaller than ±3% with few exceptions (Table 5.7.1).

Measurements of the TSI sensor internal to the SUV-150B were not always correctly recorded. Defective data were not removed from the published databases but can be easily discerned as these readings are typically constant over the course of one day.

The Eppley PSP pyranometer (S/N 32760F3) installed next to the SUV-150B was returned to Eppley for calibration when the rest of the system was in temporary storage (6/19/09 - 7/31/09). PSP data of Volume 18 were calibrated with a factor of 8.04 V/(W m^{-2}), which was established by Eppley on 4/24/07. Data of Volumes 19 and 20 have a calibration factor of 7.94 V/(W m^{-2}), which was established by Eppley on 7/30/2009.

A total of 5644 and 17494 scans are part of the Summit Volume 19 and 20 datasets, respectively.

5.7.1. Irradiance Calibration

The on-site irradiance standards used during the reporting period were the lamps 200W027, 200W030, and 200W043. Lamp 200W017 served as traveling standard at the season "opening" site visit.

Calibration history of on-site standards 200W027 and 200W030
Lamps 200W027 and 200W030 were originally calibrated on 3/28/01 by Optronic Laboratories. Both lamps were recalibrated against lamp 200W017 using "closing" scans performed at Summit on 7/11/07. These calibrations were used for processing solar data of the Volume 16 period. Lamp 200W027 was temporarily moved to San Diego and was recalibrated in March 2008 against lamps 200W028 and 200W022. This calibration was used for solar data of the reporting period. Lamp 200W030 was recalibrated in June 2009 against 200W017 using "closing" scans of the Volume 18 period, which were performed at Summit on 6/19/09. This calibration was used for solar data of the reporting period. Lamp 200W043 was calibrated on 6/2/07 against a set of four FEL lamps as described below.

Lamp 200W022 (which was used for recalibration of lamp 200W027) is one of BSI's long-term standards and is rarely used. It was calibrated by Optronic Laboratories on 3/28/01. Lamp 200W028 is the San Diego site standard.

Calibration history of traveling standard 200W017 and on-site standard 200W043
Lamps 200W017 and 200W043 were calibrated in June 2007 at BSI with four 1000-Watt FEL lamps provided by the Central UV Calibration Facility (CUCF) at Boulder. This calibration procedure was complicated by the fact that the irradiance scale of the four FEL lamps refers to the detector-based scale of the National Institute of Standards and Technology established in 2000 (NIST2000; *Yoon et al*., 2002), whereas all solar data of the NSF UVSIMN refer to the source-based NIST scale from 1990 (NIST1990,

Walker et al., 1987). The NIST2000 scale is about 1.3% larger than the NIST1990 scale. Data of certificates issued by the CUCF were converted to the NIST1990 scale before the calibration was transferred to the two lamps.

Figure 5.7.1 shows a comparison of lamps 200W027, 200W030, and 200W043 with lamp 200W017 performed on 6/19/09. The three lamps are consistent with the traveling standard to within ±1%. This a very good result considering that all lamps, with the exception of 200W030, have independent calibration trails. The three site standards were also compared with each other on 11/8/09 and 2/15/10. The lamps agreed to within ±1.0% on both occasions.

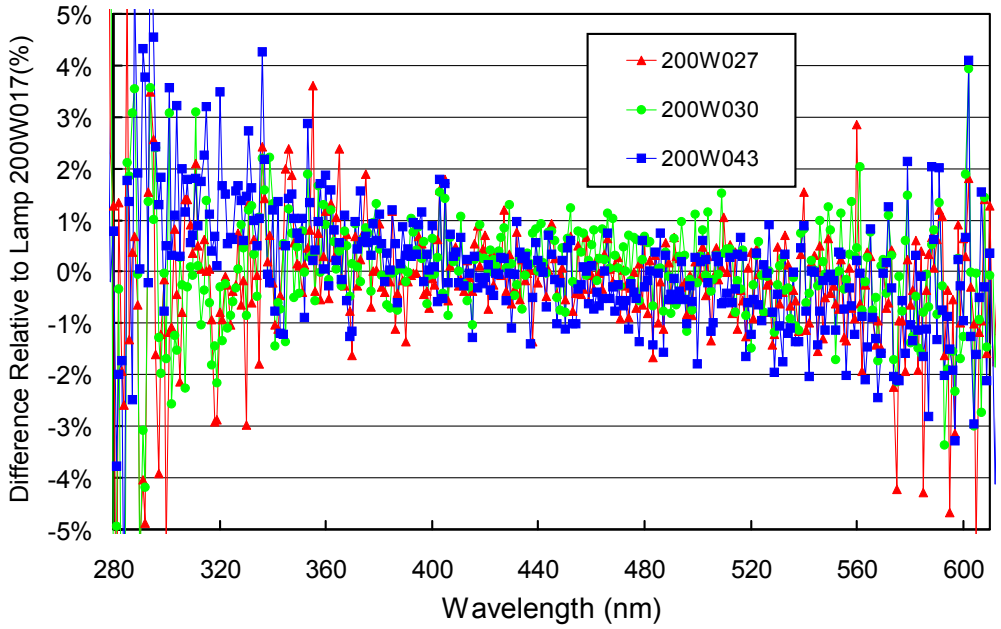

Figure 5.7.1. *Comparison of lamps 200W027, 200W030, 200W043 with lamp 200W017. Data was collected during the site visit in June 2009.*

5.7.2. Instrument Stability

The temporal stability of the spectroradiometer is monitored with bi-weekly calibrations utilizing site irradiance standards; daily response scans of the internal irradiance reference lamp; measurements of filtered photodiodes integral to the instrument's integrating sphere; and by comparison with the co-located GUV-511 radiometer and results from a radiative transfer model. Daily response scans help to uncover instabilities related to monochromator and PMT but cannot be used to track changes in the instrument's cosine collector (integrating sphere + PTFE diffuser). In contrast, the sphere's photodetectors are only sensitive to changes in the cosine collector and are not affected by possible drifts of other system components such as the optical fiber or the monochromator.

The stability of the cosine collector was determined by analyzing the signal of the sphere's photodetectors when executing absolute scans with lamps 200W027 and 200W030. Signals should ideally be constant from one calibration event to the next as the lamps were very stable. Figure 5.7.2 shows signals of the four detectors as a function of time. Data were normalized to signals recorded during the first absolute scan of each of the two lamps. Results indicate that the throughput of the collector is less in winter than in summer. The annual variation is stronger at shorter wavelengths. A similar pattern has also been observed in data of earlier volumes. We attribute these partially reversible drifts to changes in the reflectivity of the integrating sphere's wall, but the detailed mechanism is still unknown. The throughput is generally smaller during the

darkest part of the year, indicating that the changes may be caused by light sensitization. Results are consistent with the analysis of absolute scans (Figures 5.7.4.a - 5.7.4.d), excluding the possibility that drifts are caused by changes in the sensitivity of the photodetectors. Changes of the sphere's throughput are generally well predictable and could be corrected.

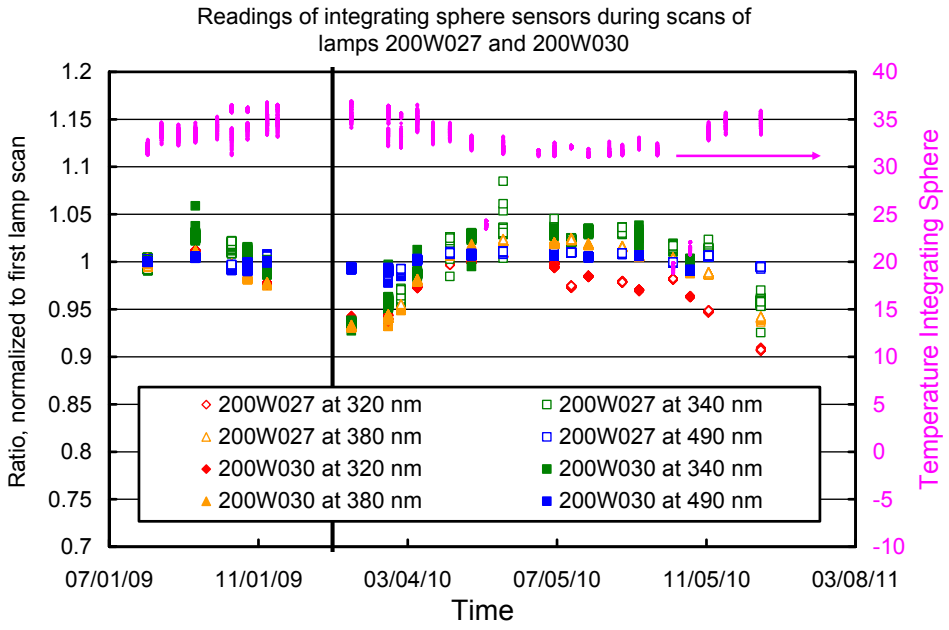

Figure 5.7.2. *Analysis of change in throughput of the instrument's integrating sphere. Change was assessed by analyzing data of photodetectors that are mounted around the sphere's exit port. Signals of the detectors were recorded during absolute scans with lamps 200W027 and 200W030. Measurements are normalized to the median of data recorded during the first absolute scans for each of the two lamps. The beginning of 2010 is indicated by a vertical line.*

Figure 5.7.3 shows changes in TSI readings and PMT currents at 320 and 400 nm, derived from response scans performed between 2/14/06 and 1/9/11. TSI measurements changed by about 10% between 2/14/06 and 6/20/09. The lamp failed and the end of August 2009 and was replaced. Data recorded after this time were scaled downward by a constant factor. The relative change of the second lamp's intensity as recorded by the TSI between 9/2/09 and 1/9/11 is similar to that of the original lamp. The trend of PMT currents follows that of the TSI measurements but superimposed on the general trend is a sinusoidal variation with a periodicity of one year. The highest PMT sensitivity is observed in mid-February of every year, while the lowest sensitivity is observed in August. We attribute this periodicity to a long-term memory of the PMT to the radiation levels it has "seen" during the months prior to the measurement. During the period of winter darkness, the PMT becomes more sensitive, and during the summer months its sensitivity decreases. As the variation is very predictable, it can be well corrected during data processing.

To account for changes of the system's sphere-throughput and PMT-sensitivity, the reporting period was broken into 22 sub-periods and a different irradiance spectrum was applied to the internal lamp in each period. A summary of the calibration periods is provided in Table 5.7.1. The ratio of these irradiance spectra relative to the spectra applied in periods P2, and P8 are shown in Figures 5.7.4.a and 5.7.4.b, respectively.

Table 5.7.1. Calibration periods for Summit Volumes 19 and 20.

Period name	Period range	Number of absolute scans	Remarks
P1	07/31/09 - 08/31/09	7	Failure of response lamp after this period
P2	09/01/09 - 10/03/09	2	
P2B	10/04/09 - 10/13/09	0	Average of P2 and P3
P3	10/14/09 - 10/31/09	2	
P4	11/01/09 - 11/12/09	3	
P4B	11/13/09 - 11/20/09	0	Average of P5 and P5
P5	11/21/09 - 12/02/09	1	
P6	12/03/09 - 12/31/09	1	
P7	01/01/10 - 01/31/10	1	
P8	02/01/10 - 02/16/10	3	
P9	02/17/10 - 03/01/10	1	
P9B	03/02/10 - 03/06/10	0	Average of P9 and P10A
P10A	03/07/10 - 03/18/10	1	
P10B	03/19/10 - 03/31/10	1	
P11	04/01/10 - 05/07/10	3	
P11B	05/08/10 - 05/20/10	0	Average of P11 and P12A
P12A	05/21/10 - 06/26/10	3	
P12B	06/27/10 - 07/09/10	2	
P13	07/10/10 - 10/01/10	6	
P14	10/02/10 - 11/13/10	3	
P14B	11/14/10 - 12/04/10	0	P14, scaled upward by 1-2%
P14B	11/14/10 - 12/04/10	0	P14, scaled upward by 1-2%

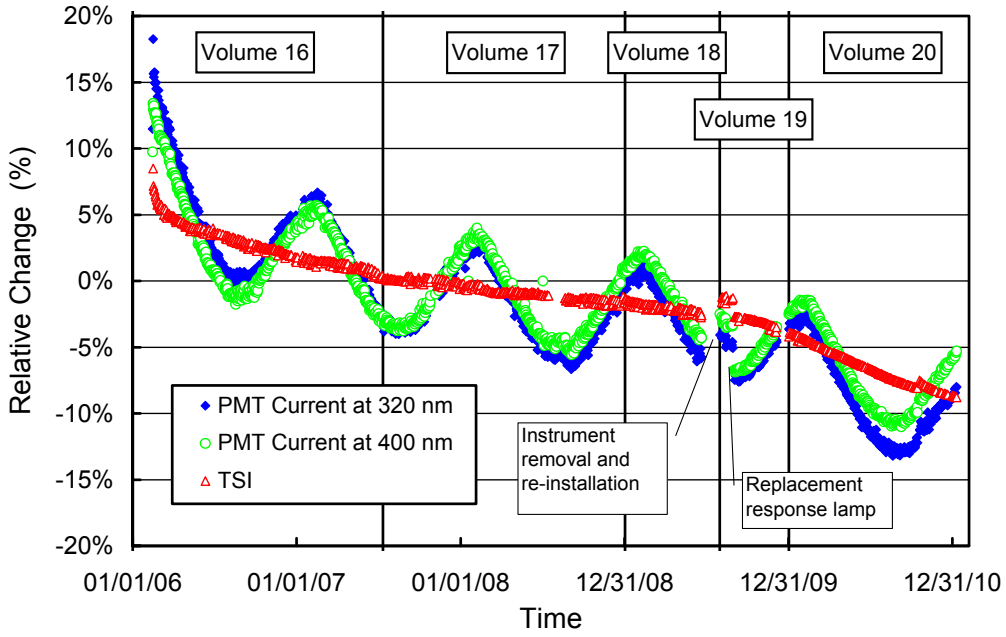

Figure 5.7.3. *Time-series of TSI signal and PMT currents at 320 and 400 nm during measurements of the internal reference lamp performed at Summit between 2/15/06 and 1/9/11. Data from 9/2/10 (date of response lamp replacement) were scaled to downward to fit into the existing pattern.*

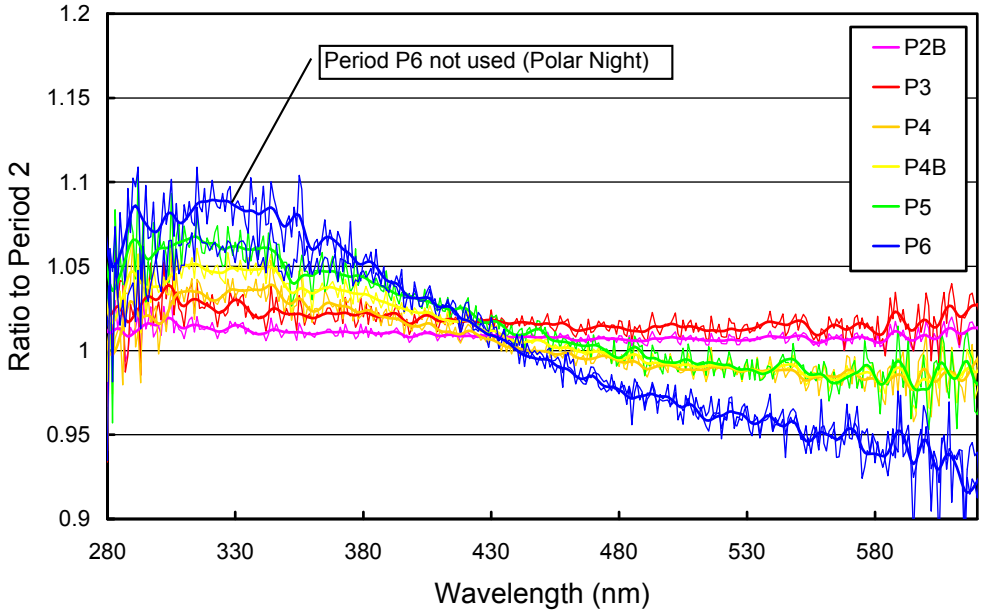

Figure 5.7.4.a *Ratios of irradiance assigned to the internal reference lamp in Periods P2B – P6, referenced to the irradiance of Period P2. Data cover the period 9/1/09 - 12/31/09 (Volume 19).*

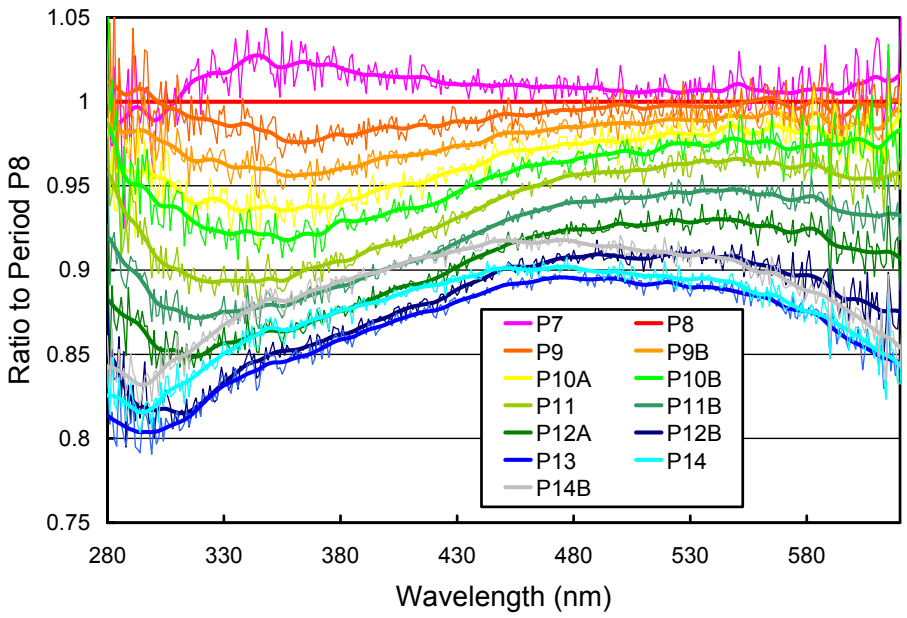

Figure 5.7.4.b *Ratios of irradiance assigned to the internal reference lamp in Periods P7 – P14B, referenced to the irradiance of Period P8. Data cover the period 1/1/10 - 12/4/10.*

The quality of calibrated solar measurements of the SUV-150B was further assessed by comparison with the GUV-511 radiometer. Figures 5.7.5.a (Volume 19) and 5.7.5.b (Volume 20) show the ratio of measurements of the GUV's 340 nm channel to measurements of the SUV-150B. The latter have been weighted with the spectral response function of the GUV's channel prior to forming the average. Measurements of the two instruments agree to within ±5%. The standard deviation of the ratio is 1.6%.

Step-changes at times when the SUV's calibration was changed are typically smaller than 2.5%. Periods when the uncertainty of SUV data is increased due to changes in the instrument's responsivity are generally those periods when the ratio of GUV/SUV at 340 nm exceeds ±3%. These periods are also indicated in Table 5.7.1. Uncertainties in the visible are smaller than in the UV due to the spectral pattern of changes in the sphere throughput.

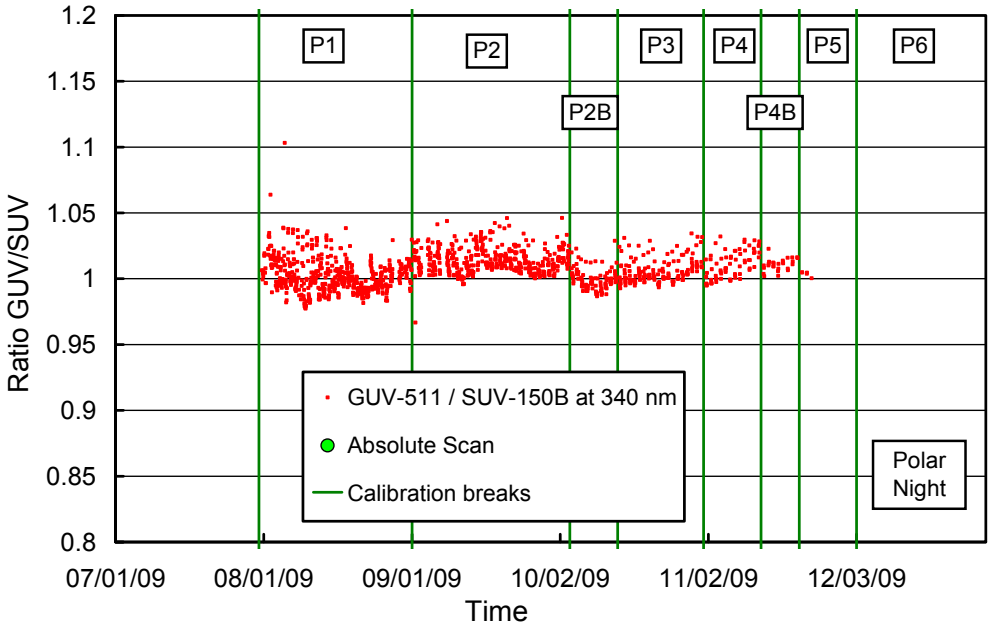

Figure 5.7.5.a. *Ratios of GUV-511 and SUV-150B measurements at 340 nm for period of Volume 19 data (2009).*

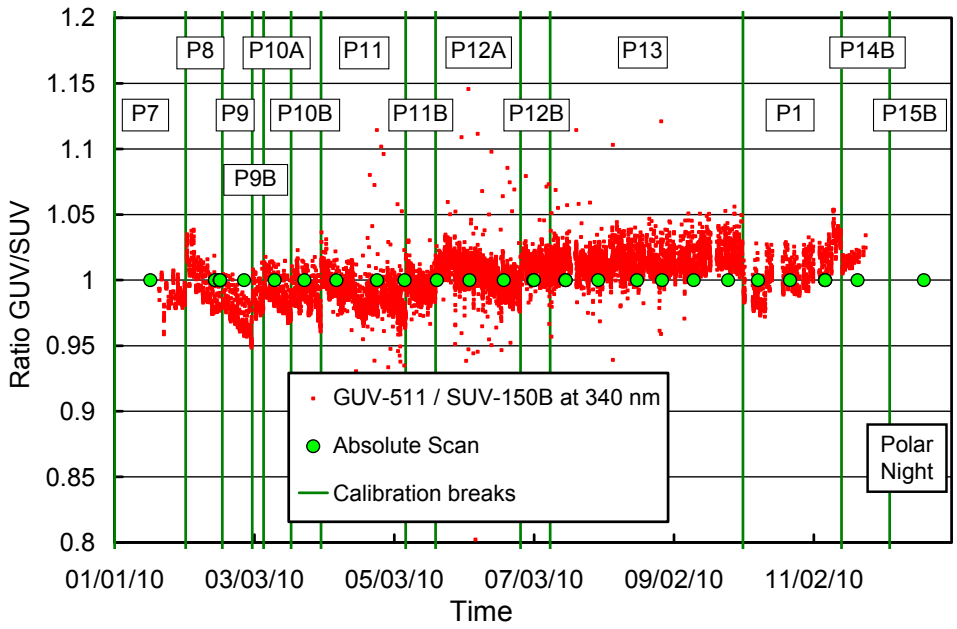

Figure 5.7.5.b. *Ratios of GUV-511 and SUV-150B measurements at 340 nm for period of Volume 20 data (2010).*

5.7.3. Wavelength Calibration

Wavelength stability of the system was monitored with the internal mercury lamp. Figure 5.7.6 shows the differences in the wavelength offset of the 296.73 nm mercury line between pairs of consecutive wavelength scans for the period 7/30/09 –12/31/10. In total, 463 scans were evaluated. For 94.8% of the scans is the difference in the wavelength offset to neighboring scans less than ±0.0055 nm. Minimum and maximum shifts between consecutive scans were -0.025 and +0.034 nm, respectively. Pairs were changes of larger than ±0.01 nm were mostly observed between 7/30/09 and 8/11/09. Note that this stability is a factor of 10 better than the wavelength stability of SUV-100 spectroradiometers. The SUV-150B has a superior wavelength stability due to the use of high-resolution optical encoders that are used in a closed feedback loop with the stepper-motor controllers.

After the data was corrected for day-to-day wavelength fluctuations, the wavelength-dependent bias between this homogenized data set and the correct wavelength scale was determined with the Fraunhofer-line correlation method used for Version 2 processing (*Bernhard et al., 2004*; see also Section 4.2.2.2). Due to the good wavelength stability of the system, only one correction function had to be applied for the entire reporting period. This function is shown in Figure 5.7.7. Since the positions of the monochromator's gratings are determined by optical encoders, irregularities in the monochromator drive are inconsequential. This explains the smoothness of the function. Most of the variations observed are artifacts of the correlation algorithm, which has an uncertainty of about 0.015 nm.

After data was corrected using this function, the wavelength accuracy of all noontime scans was verified with the "Version 2" Fraunhofer-line correlation algorithm. The results are shown in Figure 5.7.8 for four UV wavelengths and one wavelength in the visible. Residual shifts are typically smaller than ±0.03 nm.

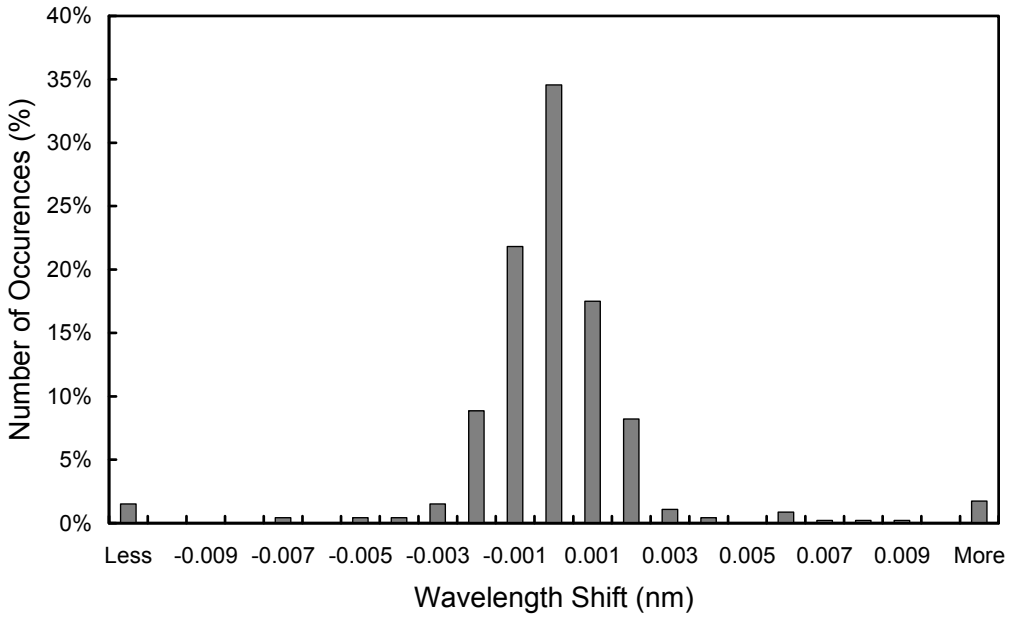

Figure 5.7.6. *Differences in the measured position of the 296.73 nm mercury line between consecutive wavelength scans for the period 7/30/09 –12/31/10. The labels of the horizontal axis give the center wavelength shift for each column. The 0-nm histogram column covers the range from -0.0005 to +0.0005 nm. "Less" means shifts smaller than -0.0105 nm; "more" means shifts larger than 0.0105 nm.*

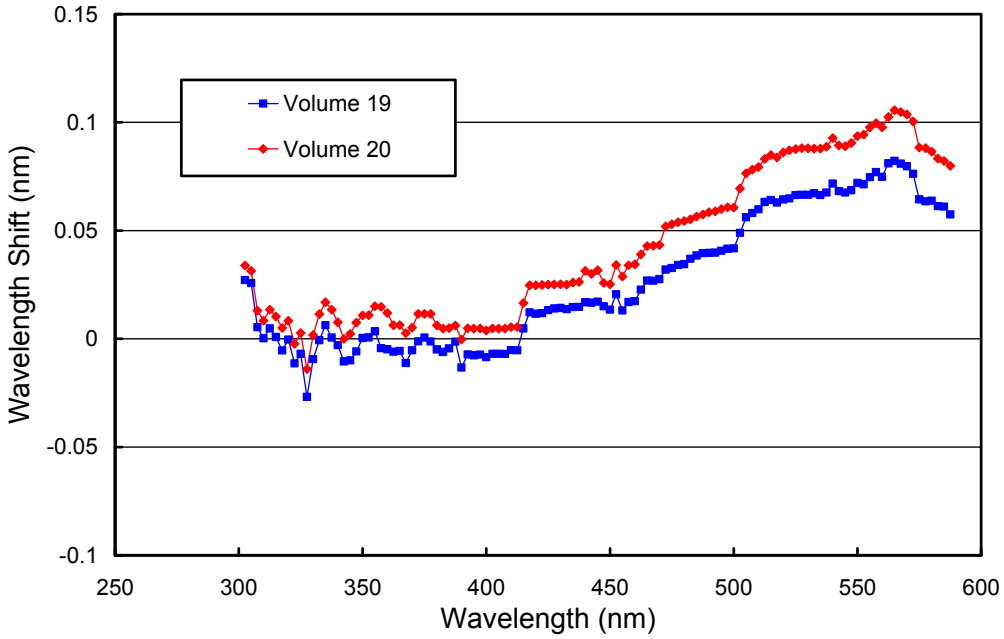

Figure 5.7.7. *Monochromator non-linearity correction functions for Volume 19 and 20 periods at Summit.*

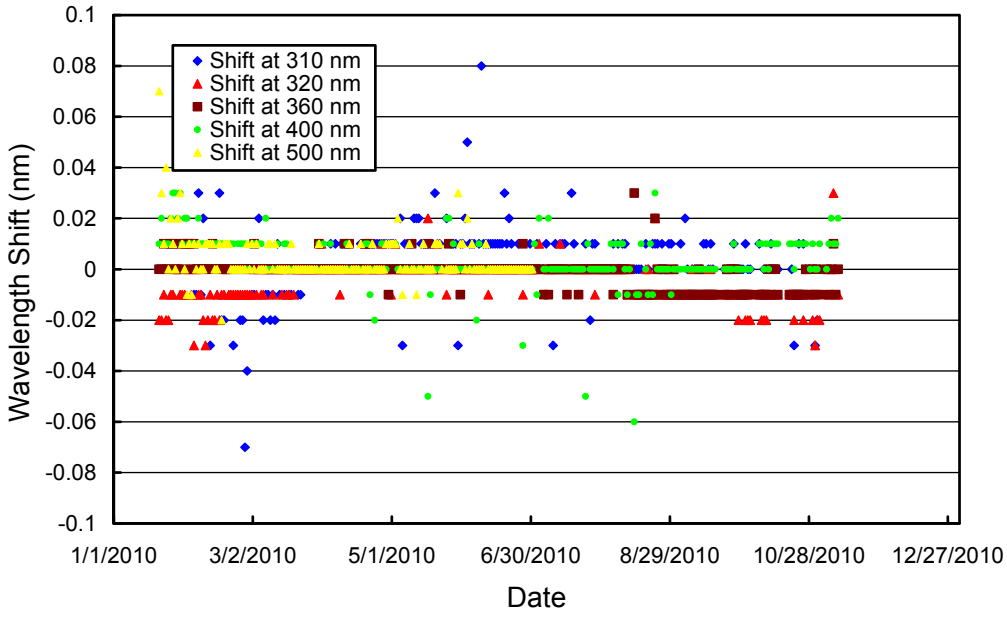

Figure 5.7.8. *Wavelength accuracy check of final Volume 20 data at five wavelengths in the UV and visible by means of Fraunhofer-line correlation. All noontime measurement have been evaluated.*

5.7.4. Missing Data

A total of 23138 scans are part of the Summit Volume 19 and 20 datasets. Missing periods are summarized in Table 5.7.2.

Table 5.7.2. Incomplete days in the Summit Volume 19 and 20 datasets.

Period	Reason
05/23/10	Unknown
07/04/10	Software error
08/02/10	Unknown
09/03/10	Software error
09/18/10 - 09/19/10	Software error
10/03/10 - 10/5/10	Software error
10/15/10 - 10/18/10	Power outage
10/27/10	Unknown
11/02/10 - 11/03/10	Software error

5.7.5. GUV Data

The GUV-511 radiometer, which is installed next to the SUV-150B, was calibrated against final SUV-150B measurements following the procedure outlined in Section 4.3.1, separately for Volumes 19 and 20. From the calibrated measurements, data products were calculated (Section 4.3.2). Figure 5.7.9 shows a comparison of GUV-511 and SUV-150B erythemal irradiance based on final Volume 19 and 20 data. For solar zenith angles smaller than 80°, measurements of the two instruments agree to within ±1.6% (±1σ). This good agreement confirms that drifts in SUV-150B data discussed in Section 5.7.2 have been satisfactorily removed by adjusting the instrument's calibrations. We advise data users to use SUV-150B rather than GUV-511 data whenever possible, in particular for low-Sun conditions.

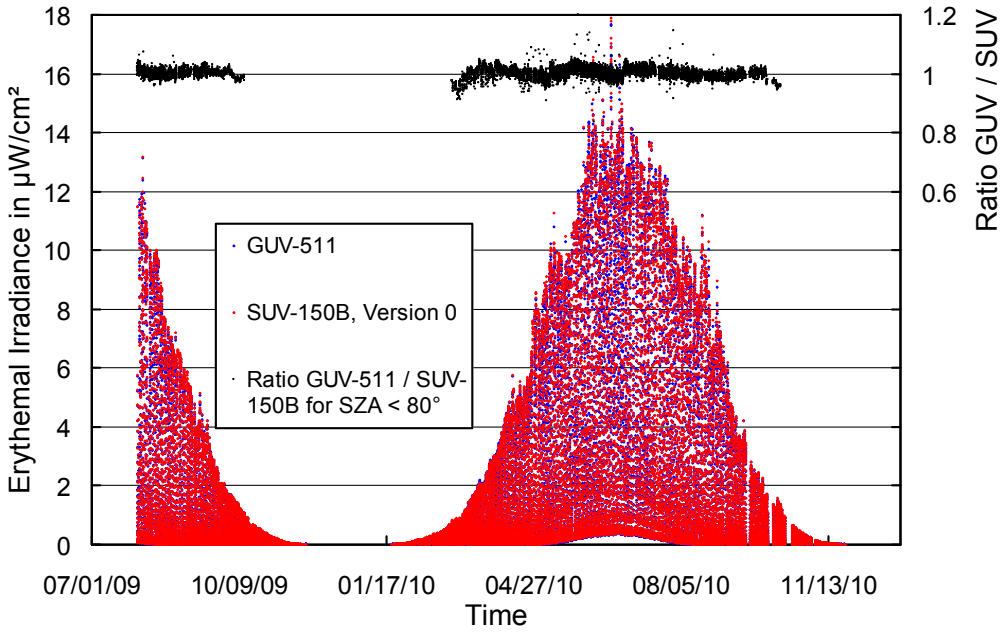

Figure 5.7.9. *Comparison of erythemal irradiance measured by the SUV-150B spectroradiometer and the GUV-511 radiometer. SUV-150B measurements are based on "Version 0" (cosine-error uncorrected) data.*

Figure 5.7.10 shows a comparison of total ozone measurements from the GUV-511, the SUV-150B (Version 2 data, available at www.biospherical.com/nsf/Version2/), and the Ozone Monitoring Instrument (OMI). GUV-511 ozone values were calculated as described in Section 4.3.3. Between May and September, GUV-511 ozone data agree almost ideally with SUV-150B and OMI measurements. GUV data are a few percent low for March, April, and October when solar elevations are small. The reason for this bias is the effect of the ozone profile on ozone retrievals. For SZA larger than 80°, measurements of the GUV's 305 nm channel are close to the detection limit. GUV ozone data at large SZAs become unreliable and should not be used.

There is generally good agreement between SUV-150B and OMI data. The average ratio SUV/OMI is 1.01, and the standard deviation of the two datasets is 3.4%. This good agreement—even at large SZAs—is achieved by using ozone profiles in the inversion algorithm, which were measured at Summit by NOAA/ESRL.

The average ratio GUV / OMI is 0.996 and the standard deviation of the ratio is 3.5% The graph also indicates a period when OMI data are unrealistically high. This observation can likely be related to some instrumental problems of OMI.

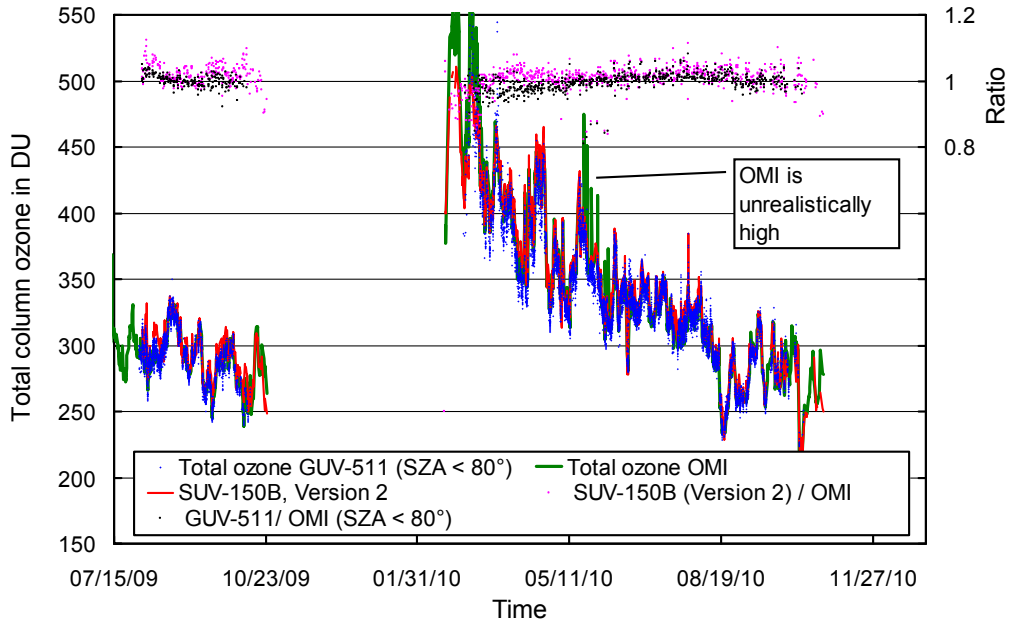

Figure 5.7.10. *Comparison of total column ozone measurements from GUV-511, SUV-150B (Version 2 data), and OMI. GUV-511 measurements are plotted in 15 minute intervals. For calculating the ratio of data sets, only measurements concurrent with the OMI overpass were evaluated.*